Macrophages sense and kill bacteria through carbon monoxide–dependent inflammasome activation

Barbara Wegiel,[1] Rasmus Larsen,[2] David Gallo,[1] Beek Yoke Chin,[1] Clair Harris,[1] Praveen Mannam,[3] Elzbieta Kaczmarek,[4] Patty J. Lee,[3] Brian S. Zuckerbraun,[5] Richard Flavell,[3,6] Miguel P. Soares,[2] and Leo E. Otterbein[1]

[1]Department of Surgery, Transplant Institute, Beth Israel Deaconess Medical Center (BIDMC), Harvard Medical School, Boston, Massachusetts, USA. [2]Instituto Gulbenkian de Ciência, Oeiras, Portugal. [3]Yale University School of Medicine, Department of Immunobiology, New Haven, Connecticut, USA. [4]Center for Vascular Biology, Department of Surgery, BIDMC, Harvard Medical School, Boston, Massachusetts, USA. [5]University of Pittsburgh Medical Center, Pittsburgh, Pennsylvania, USA. [6]Howard Hughes Medical Institute, New Haven, Connecticut, USA.

Microbial clearance by eukaryotes relies on complex and coordinated processes that remain poorly understood. The gasotransmitter carbon monoxide (CO) is generated by the stress-responsive enzyme heme oxygenase-1 (HO-1, encoded by *Hmox1*), which is highly induced in macrophages in response to bacterial infection. HO-1 deficiency results in inadequate pathogen clearance, exaggerated tissue damage, and increased mortality. Here, we determined that macrophage-generated CO promotes ATP production and release by bacteria, which then activates the Nacht, LRR, and PYD domains-containing protein 3 (NALP3) inflammasome, intensifying bacterial killing. Bacterial killing defects in HO-1–deficient murine macrophages were restored by administration of CO. Moreover, increased CO levels enhanced the bacterial clearance capacity of human macrophages and WT murine macrophages. CO-dependent bacterial clearance required the NALP3 inflammasome, as CO did not increase bacterial killing in macrophages isolated from NALP3-deficient or caspase-1–deficient mice. IL-1β cleavage and secretion were impaired in HO-1–deficient macrophages, and CO-dependent processing of IL-1β required the presence of bacteria-derived ATP. We found that bacteria remained viable to generate and release ATP in response to CO. The ATP then bound to macrophage nucleotide P2 receptors, resulting in activation of the NALP3/IL-1β inflammasome to amplify bacterial phagocytosis by macrophages. Taken together, our results indicate that macrophage-derived CO permits efficient and coordinated regulation of the host innate response to invading microbes.

Introduction

Innate immune cells have a large array of defense mechanisms to handle bacterial infection. These are triggered upon recognition of pathogen-associated molecular patterns (PAMPs) by pattern recognition receptors (PRR), i.e., innate receptors (1, 2), including the Nacht, LRR and PYD domains-containing protein 3/NOD-like receptor family, pyrin domain-containing 3 (NALP3/NLRP3) inflammasome (3–8). Recently defined danger-associated molecular patterns (DAMPs) have also been associated with additional signals leading to activation of the NALP3 inflammasome and IL-1β secretion (3, 9, 10), allowing for rapid recruitment and activation of phagocytes (3, 11–13). DAMPs include intracellular host proteins, such as heat shock proteins (14), high-mobility group box 1 (HMGB1) (15), and hyaluron fragments (16) as well as nonprotein molecules including ATP (7), uric acid (17), and DNA (18).

IL-1β secretion in response to PRR engagement requires caspase-1 activation, which cleaves pro–IL-1β into its active mature secreted form (4, 10). Caspase-1–deficient mice are more susceptible to *E. coli* infection than WT mice (19). NALP3 inflammasome (3–7) plays a critical role in the activation of caspase-1 in response to a variety of agonists, including bacterial toxins such as nigericin and mycotoxin as well as silica, asbestos, amyloid β, hemozoin, and extracellular ATP (20, 21). While it is clear that these agonists can promote NALP3 inflammasome activation, the molecular mechanisms linking microbial recognition and phagocytosis to the NALP3 inflammasome activation are not fully understood.

ATP activates $P2X_7$ receptors, which act as potent initiators of NALP3 inflammasome and IL-1β cleavage and secretion (7, 22, 23). ATP can be released from host cells, acting as an autocrine DAMP to promote $P2X_7$, NALP3 inflammasome, and caspase-1 activation (24). Here, we provide evidence for an additional molecular mechanism underlying host-pathogen interaction whereby ATP, acting as a PAMP, is released from viable bacteria and triggers $P2X_7$, NALP3 inflammasome, and caspase-1 activation, which leads to IL-1β cleavage and secretion, thus regulating host immunity.

Heme oxygenase-1 (HO-1) is an inducible immunomodulatory (25) and cytoprotective enzyme (26–28) whose fundamental purpose is the degradation of heme to biliverdin, carbon monoxide (CO), and free iron (29). HO-1 confers protection against a variety of pathologic conditions, including endotoxic shock and bacterial sepsis (25, 30–37). While CO appears to mediate many of the salutary effects of HO-1 (38), its mechanism of action remains controversial. Chung et al. (32) and Desmard et al. (39) demonstrate that CO-releasing molecules (CO-RM) confer host protection against infection, improving survival and preventing end-organ failure in response to bacterial infection, an effect associated with direct bacterial clearance and killing (39, 40). When produced physiologically, however, CO has no direct

Conflict of interest: The authors have declared that no conflict of interest exists.
Submitted: July 1, 2014; **Accepted:** August 28, 2014.
Reference information: *J Clin Invest*. 2014;124(11):4926–4940. doi:10.1172/JCI72853.

effect on bacterial growth and survival unless administered exogenously at supraphysiologic conditions (39). Inhaled CO has been tested in large animals and phase I human trials and approved for use at up to 10% to 12% carboxyhemoglobin (COHb). CO at similar regimens to those defined herein is currently being evaluated in phase II trials including studies of lung disease, organ transplantation, and paralytic ileus (NCT00122694, NCT01523548, NCT00531856, NCT01050712; www.clinicaltrials.gov). Here, we propose that when produced endogenously by HO-1, CO acts as a key mediator of host defense used by the macrophages. This effect relies on the induction of ATP production and release by bacteria, regulating macrophage activation and promoting bacterial clearance and host survival via the $P2X_7$/NALP3 inflammasome and caspase-1/IL-1β signal transduction pathways.

Results

HO-1 controls bacteria-induced IL-1β expression by macrophages. Primary macrophages exposed to bacteria or endotoxin exhibit a marked increase in expression of HO-1 and proinflammatory cytokines such as IL-1β (32, 41) To test the role of HO-1 in IL-1β expression and activation in response to bacteria challenge, we used macrophages from *Hmox1*$^{-/-}$and *LyzM-Cre Hmox1*$^{fl/fl}$ mice and WT macrophages infected with retroviral HO-1 shRNA (Figure 1, A–C). Activation of IL-1β in response to bacteria was largely dependent on the presence and activity of HO-1, as macrophages lacking HO-1 expression showed no increase in cleaved IL-1β and expressed lower pro–IL-1β versus controls, as measured by immunoblot or ELISA (Figure 1, A–C). Of note, commercial ELISA kits detect pro–IL-1β and thus underestimate IL-1β processing by the NALP3 inflammasome pathway. The effects on IL-1β were specific and not explained by a global downregulation of macrophage activation in the absence of HO-1, as bacteria exposure induced a robust increase in TNF protein that was independent of HO-1 (Figure 1D). The effects of HO-1 on IL-1β were determined to be at the protein level (both the pro and cleaved forms of IL-1β). No statistical change in inflammasome component mRNA was observed between *Hmox1*$^{+/-}$ and *Hmox1*$^{-/-}$ macrophages in the presence or absence of bacteria (Figure 1E). Therefore, these data suggest that HO-1 is involved in part in regulation of IL-1β expression and processing via the inflammasome multiplex including NALP3 and the pro–IL-1β cleavage enzyme caspase-1.

To evaluate whether macrophages lacking HO-1 were deficient in their ability to activate the inflammasome, we treated macrophages with exogenous ATP, a well-characterized NALP3 stimulus. BM-derived macrophages (BMDMs) isolated from *Hmox1*$^{+/+}$ or *Hmox1*$^{-/-}$ were activated with bacterial LPS followed by treatment with ATP. LPS treatment increased pro–IL-1β expression, which was then cleaved to IL-1β with the addition of ATP in both *Hmox1*$^{-/-}$ and *Hmox1*$^{+/+}$ macrophages (Figure 1, F and G). Macrophages lacking HO-1 showed 25% to 30% less cleaved IL-1β compared with WT cells, which was in part related to there being less pro–IL-1β. While *Hmox1*$^{-/-}$ BMDMs respond to LPS plus ATP with a significant increase in pro–IL-1β, they have been shown to also exhibit a delay in differentiation and are therefore less responsive to LPS due to lower expression of CD14 (42). Collectively, these data suggest that ATP-dependent macrophage activation is in large part independent of HO-1, but indicate that HO-1 may play a role in IL-1β processing. The dependency of IL-1β activation on HO-1 expression in response to bacteria was corroborated pharmacologically. We saw similar effects in WT macrophages treated with tin-protoporphyrin-IX (Sn-PP-IX), which blocks HO-1 and HO-2, as well as the highly HO-1–selective inhibitor QC-15 (ref. 43 and Figure 2A).

CO modulates IL-1β activation and substitutes for HO-1. HO-1 generates biologically active CO that not only imparts antiinflammatory effects, but also augments immune responses against pathogens (44). We therefore next tested whether administration of exogenous CO could rescue HO-1 deficiency and reestablish the IL-1β response. Administration of exogenous CO to macrophages treated with the selective inhibitors of HO-1 was as follows: Sn-PP-IX or QC-15 or macrophages harvested from *LyzM-Cre Hmox1*$^{fl/fl}$ restored IL-1β secretion in response to bacteria in the presence of *E. coli* (Figure 2, A and B). Moreover, WT cells (either BMDMs or primary peritoneal macrophages [PMs]) showed an enhanced response to CO treatment with significantly greater IL-1β expression and caspase-1 activation compared with air-treated controls, suggesting that CO targeted in part the inflammasome machinery that generates active IL-1β (Figure 2C). We also tested an intracellular pathogen, *Salmonella typhimurium*, which mediates IL-1β secretion via a NALP3 inflammasome–independent pathway and observed no difference in IL-1β secretion in *Hmox1*$^{+/+}$ and *Hmox1*$^{-/-}$ macrophages, further suggesting that CO produced by HO-1 specifically targets the NALP3 inflammasome pathway (Supplemental Figure 1A; supplemental material available online with this article; doi:10.1172/JCI72853DS1). Further, biliverdin, the other product of HO-1 activity, had no effect on bacteria-induced IL-1β expression (Supplemental Figure 1B). Finally, the effects of CO, like those observed with HO-1, were specific to IL-1β and not explained by global modulation of macrophage function because treatment with CO had no therapeutic effect on bacteria-induced TNF expression (Figure 2D).

HO-1 and CO are important in bacteria killing by macrophages. We next sought to study whether the effects of HO-1 and CO on IL-1β resulted in a functional effect on macrophage bacterial killing. IL-1β has been shown to influence bacterial phagocytosis (45). Bacterial killing was impaired in macrophages lacking HO-1 as expected, an effect rescued by administration of exogenous CO (Figure 3A). Initial experiments employed the well-characterized model of bacterial clearance in which bacteria growth is controlled by the addition of antibiotics. We found that addition of antibiotics 2 hours after infection to eliminate extracellular bacteria further amplified CO effects, with more rapid bacterial processing and less intracellular bacteria viability (Figure 3B). All subsequent experiments therefore were performed in the absence of antibiotics, which we considered a stronger correlate with our in vivo sepsis models where no antibiotics were used. The effects of CO on bacteria clearance were similar in mouse and primary human macrophages (Figure 3C). Strikingly, macrophages treated with CO were able to more effectively clear bacteria at concentrations that were otherwise unable to be cleared in air-treated control macrophages (Figure 3D). These effects mediated by CO were unrelated to direct bactericidal effects, as CO had no effect on bacterial growth in the absence of macrophages (Figure 3E).

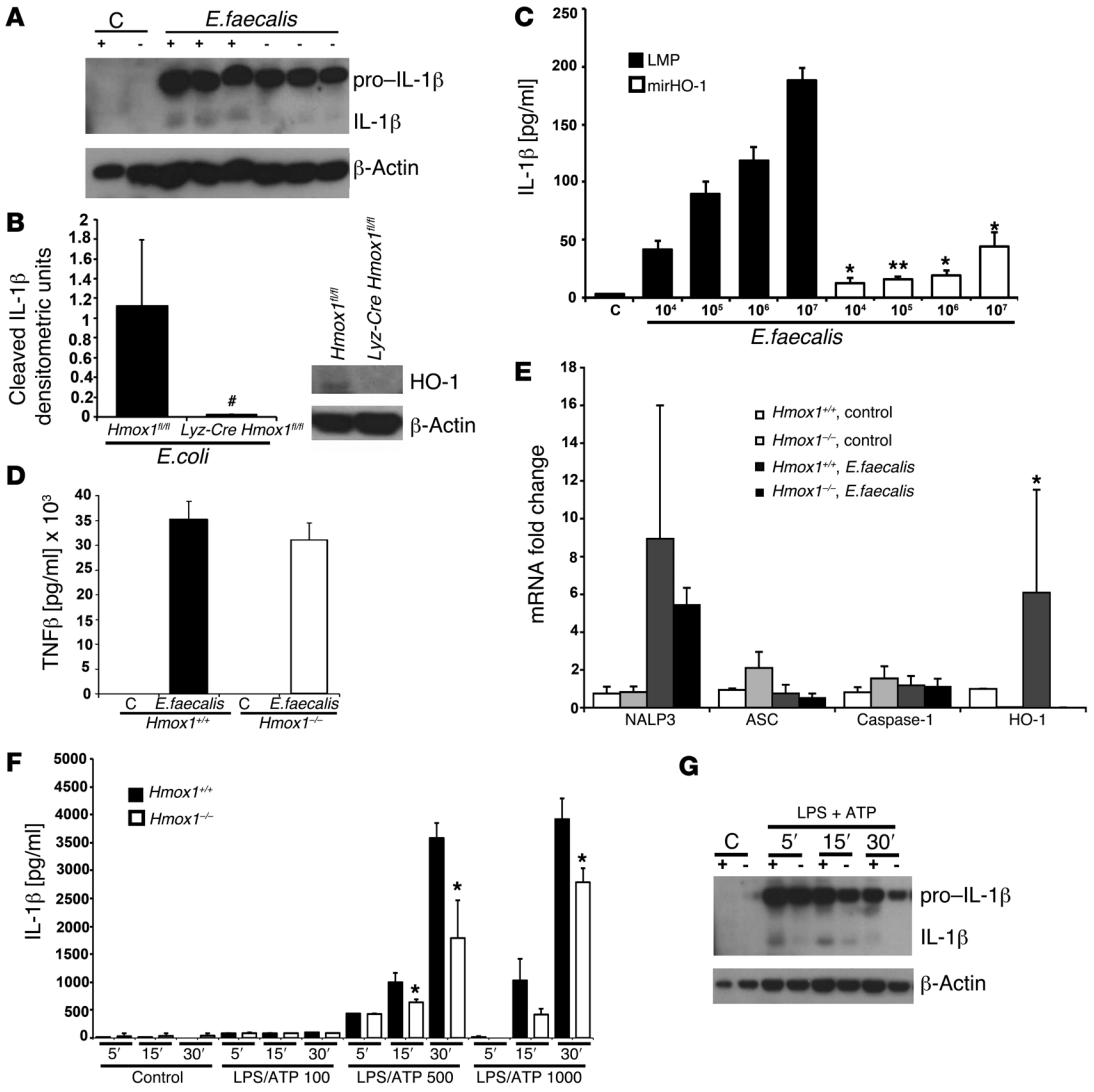

Figure 1. Role of HO-1 on IL-1β release from bacteria-infected macrophages. (**A**–**C**) Representative immunoblots and ELISA for IL-1β in BMDMs or PMs treated with indicated bacteria (10^6 CFU/ml *E. faecalis* or 10^4 CFU/ml *E. coli*) for 10 hours. (**A**) *Hmox1*$^{-/-}$ (–) and *Hmox1*$^{+/+}$ (+) BMDMs. (**B**) Immunoblot quantitation of PMs from *LyzM-Cre Hmox1*$^{fl/fl}$ and *Hmox1*$^{fl/fl}$ injected i.p. with *E. coli* for 2 hours (inset; *Hmox1* expression in naive PMs). (**C**) Retroviral shRNA against HO-1 or latent membrane potential (LMP) control in BMDMs treated as in **A**. $^{\#}P < 0.01$, *LyzM-Cre Hmox1*$^{fl/fl}$ versus *Hmox1*$^{fl/fl}$; $^{**}P < 0.001$, $^{*}P < 0.05$ versus LMP. Results represent average ± SD of 2 independent experiments in triplicate. (**D**) TNF ELISA in supernatants from BMDMs treated as in **A**. Results represent mean ± SD of 2 independent experiments in triplicate. (**E**) Real-time PCR of cDNA from cells treated as in **A**. Results represent mean fold change versus control ± SD of 2 independent experiments in triplicate. $^{*}P < 0.02$. (**F** and **G**) IL-1β ELISA and immunoblot of BMDM supernatants from *Hmox1*$^{+/+}$ and *Hmox1*$^{-/-}$ treated ± LPS (1 ng/ml) for 5 hours followed by 100 μM, 500 μM, or 1000 μM ATP. Data represent mean ± SD of n = 4–6 from 3 independent experiments. $^{*}P < 0.05$.

Macrophage viability was also not altered by CO when tested in the presence of *Enterococcus faecalis*, where we observed 97% ± 2% viability in air versus 93% + 4% in CO measured by trypan blue exclusion. Collectively, these data show that expression of HO-1 and its bioactive product CO are required in part for bacterial clearance by macrophages.

CO increases bacterial-induced IL-1β secretion and bacterial clearance by macrophages through a NALP3 inflammasome–dependent mechanism. The ability of macrophages to generate IL-1β is significantly impaired in the absence of functional NALP3 and caspase-1 (4). Macrophages harvested from both *Nalp3*$^{-/-}$ and *Casp1*$^{-/-}$ mice showed a significant impairment in ability to process and kill bacteria, which was most evident in caspase-1–deficient macrophages, suggesting at least in part that IL-1β was participating in the bactericidal function of macrophages (Figure 4, A and B). Treatment with CO was unable to augment killing in macrophages deficient in NALP3 or caspase-1 as compared with CO-treated *Nalp3*$^{+/+}$ and *Casp1*$^{+/+}$ macrophages (Figure 4, A and B). These findings further confirmed CO as promoting bacterial clearance by macrophages in part through a mechanism involving NALP3, caspase-1, and IL-1β activity. IL-1β is known to autoamplify macrophage activation in an autocrine or paracrine fashion (24, 46).

We and others have demonstrated that HO-1 deficiency results in impaired bacterial clearance (32), but provided no mechanism other then greater susceptibility to infection. The observed effects of CO on IL-1β cleavage/secretion and clearance

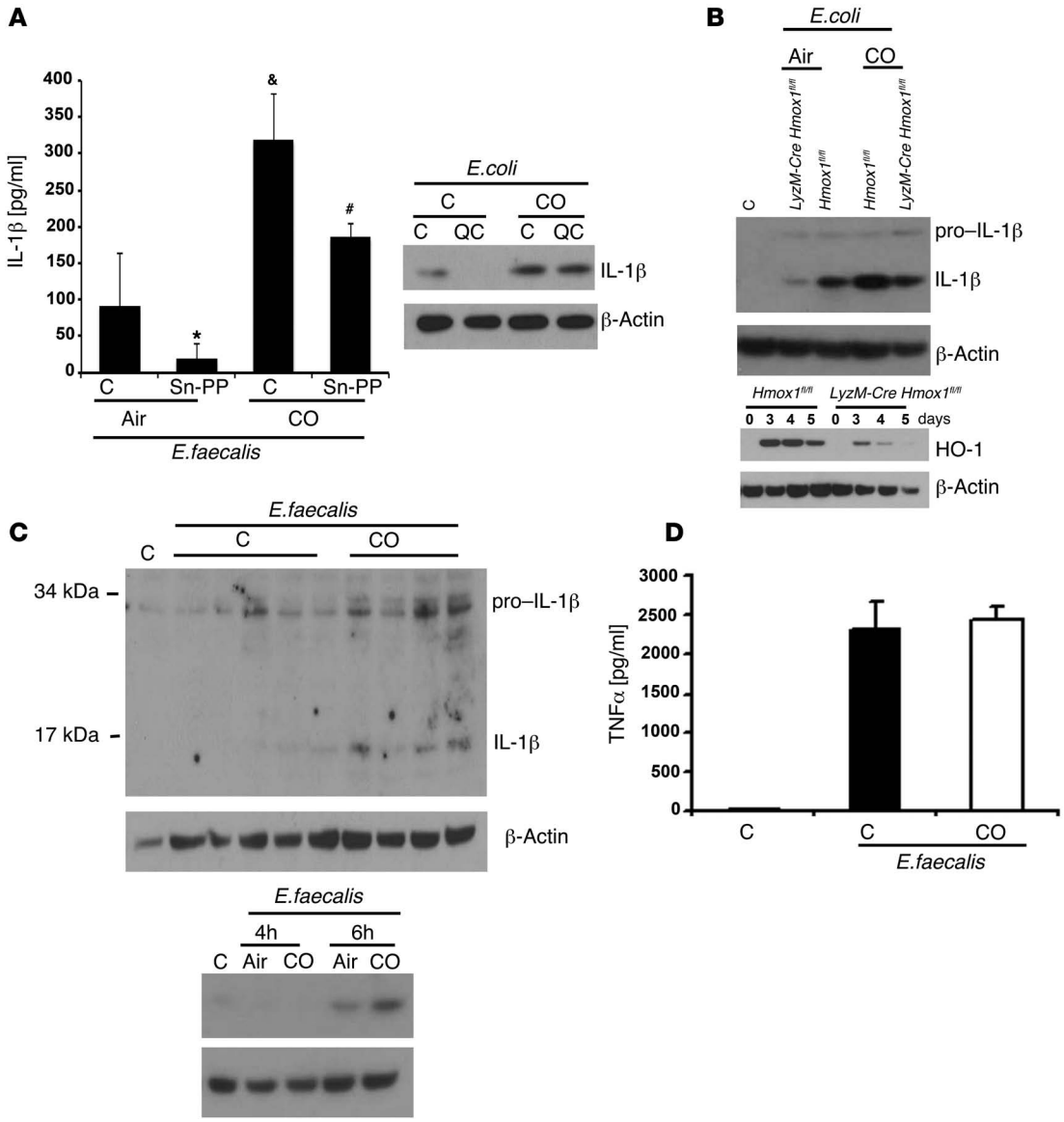

Figure 2. Role of HO-1 and CO in IL-1β activation in macrophages. (**A**) IL-1β ELISA and immunoblot in BMDMs ± selective HO-1 inhibitors Sn-PP-IX and QC-15 ± CO started 4 hours after bacteria administration (10^6 CFU/ml) for 6 hours. Note that CO reversed the loss in HO-1 activity found in air treatment. $^*P < 0.05$, air versus air + Sn-PP-IX; $^{\&}P < 0.01$, air versus CO; $^{\#}P < 0.02$, CO + Sn-PP-IX versus Sn-PP-IX. (**B**) Upper panel: IL-1β in BMDMs from the indicated mice ± *E. coli* (10^4 CFU/ml) ± CO as above. Note that CO rescues the IL-1β response in *LyzM-Cre Hmox1*$^{fl/fl}$ that is absent in air-treated controls (comparing lanes 2 and 5). Lower panel: immunoblot showing disappearance of HO-1 in *LyzM-Cre Hmox1*$^{fl/fl}$ differentiated over 5 days in response to MCSF (20 ng/ml). Note that as the Lyz promoter becomes active, HO-1 expression decreases. (**C**) Representative IL-1β and active caspase-1 p20 immunoblots in BMDMs. CO was administered for 6 hours starting 4 hours following *E. faecalis* infection (10^6 CFU/ml). (**D**) TNF ELISA in supernatants from BMDMs infected with *E. faecalis* as above. All blots represent 2 to 3 independent experiments expressed relative to β-actin as loading control. All ELISA data represent mean ± SD of 2 to 3 independent experiments in triplicate.

combined with the lack of effects in *Nalp3*$^{-/-}$ and *Casp1*$^{-/-}$ macrophages prompted us to next test whether the enhanced IL-1β cleavage/secretion was participating in the effect exerted by CO on bacterial phagocytosis and/or clearance. The notion that CO promotes bacteria clearance via a mechanism that relies on IL-1β cleavage/activation was tested and reinforced by the observation that addition of recombinant IL-1β dose dependently increased *E. faecalis* clearance by macrophages similar to that observed with CO (Figure 4C). Further, the effect of CO on bacterial killing was abrogated using an anti–IL-1β neutralizing antibody (Figure 4C). It is therefore likely that IL-1β acts on macrophages in an autocrine manner, as we also observed an increase in IL-1β receptor expression in *E. coli*–treated macrophages (Figure 4D). Given that CO exposure was initiated hours after bacteria administration, we elected not to focus on TLR receptors as potential mechanisms of action and targets for CO. Additionally, there was a significant reduction in bacteria-elicited IL-1β expression in BMDMs from *Tlr2*$^{-/-}$ and *Tlr4*$^{-/-}$ mice likely due to deficiencies in their ability to respond appropriately to bacteria wall components, resulting in less pro–IL-1β induction (47–49).

CO requires the presence of nucleotides to increase IL-1β in macrophages. Efforts to delineate the mechanism by which CO induces

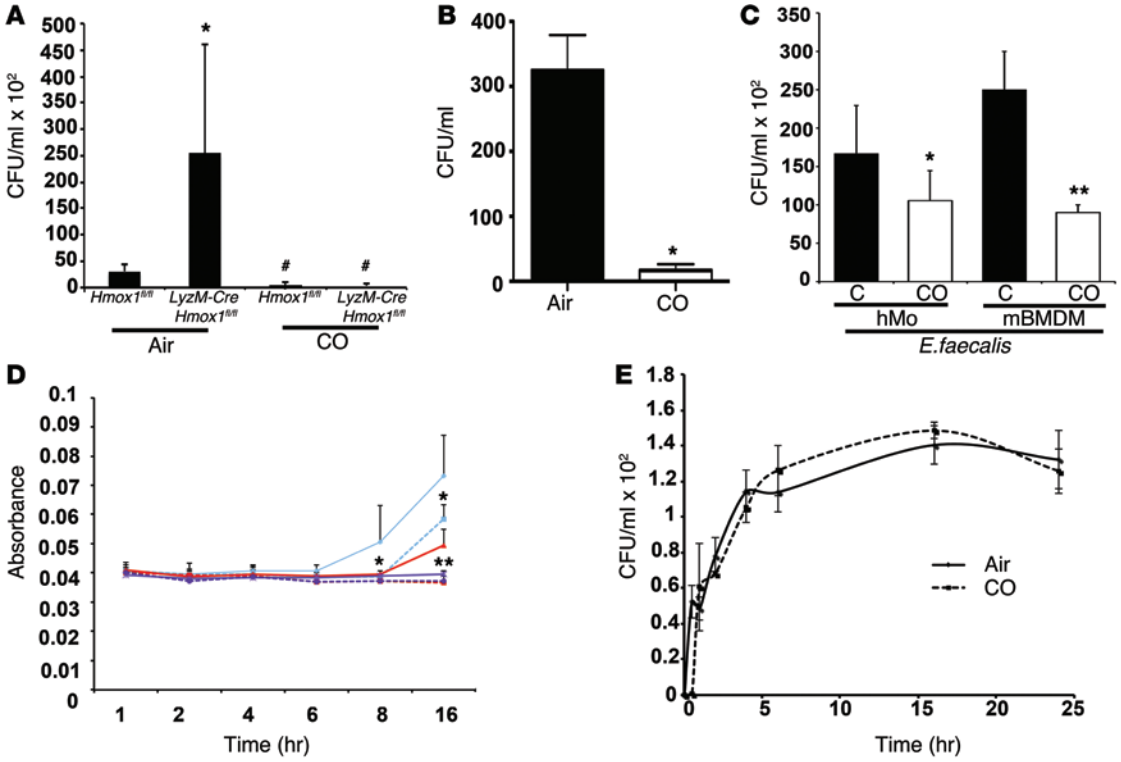

Figure 3. CO enhances bacterial killing by macrophages. (**A**) CFU in BMDM lysates ± *E. coli* (10^4) administered for 1 hour followed by exposure to CO or air for 6 hours. $^{\#}P < 0.05$, CO versus air in *LyzM-Cre Hmox1*$^{fl/fl}$ and *Hmox1*$^{fl/fl}$ macrophages; $^{*}P < 0.05$, *LyzM-Cre Hmox1*$^{fl/fl}$ versus *Hmox1*$^{fl/fl}$ macrophages. (**B**) Bacterial counts in BMDM lysates ± *E. coli* administered for 2 hours followed by addition of penicillin/streptomycin ± CO for 6 hours. Results represent average ± SD of 2 independent experiments in triplicate. $^{*}P < 0.001$, CO versus air. (**C**) CFU in supernatants of mouse BMDMs or primary human peripheral blood monocytes (hMo) + *E. faecalis* (10^6) for 1 hour prior to CO (white bars) or air (black bars) administration for an additional 4 hours. $^{*}P < 0.007$; $^{**}P < 0.01$, CO versus air (C). (**D**) Growth kinetics of *E. faecalis* in BMDM supernatants ± CO measured as absorbance at 600 nm. Blue indicates 10^2, red indicates 10^6, and violet indicates 10^{10} CFU/ml. CO, dotted lines; air, solid lines. Data represent mean ± SD of $n = 3$/group/time point. $^{*}P < 0.005$; $^{**}P < 0.05$, versus air at the same bacterial concentration and time point. (**E**) Growth kinetics of *E. faecalis* in the medium in the presence or absence of CO. Results represent mean ± SD from 3 independent experiments. Note: similar effects of CO on growth were observed with *E. coli*.

IL-1β cleavage/activation and bacterial clearance directed us initially to test the effect of CO on well-established activators of the NALP3 inflammasome. CO can induce mitochondrial ROS generation in macrophages, an effect that could enable NALP3 inflammasome activation (50–52). *E. faecalis* induced a modest but significant ROS generation in macrophages, an effect that was not further modulated by CO (Supplemental Figure 2, A and B). This suggested to us that the mechanism by which CO modulates the NALP3 multiplex activation does not involve modulation of ROS production in bacteria-treated macrophages (52). It is likely, however, that the elevated ROS do contribute to bacterial killing in the lysosomal compartment. Inhibition of cathepsin B, a protease known to activate NALP3 inflammasome, also did not modulate CO-induced IL-1β cleavage/secretion (Figure 4E).

Somewhat surprisingly, the effects of CO were dependent on the presence of ATP as well as on a functional cytoskeletal apparatus. We augmented ATP catalysis using apyrase and used cytochalasin B to block actin microfilament formation, and both of these agents suppressed the ability of CO to induce IL-1β secretion (Figure 4E). Remarkably, neither apyrase nor the cytochalasin B inhibitor completely returned IL-1β to basal levels in air-treated controls, suggesting other mechanisms in place, including elevated expression of pro–IL-1β. These data corroborate the effects of CO on macrophage lysosomal activity, in which CO exposure increased the number of bacteria contained in lysosomes (Figure 4B).

CO induces active release and production of ATP from bacteria. The requirement for ATP generation in the CO response directed us to first study whether the macrophages were the source for increased ATP. We observed that CO had no effect on intracellular ATP production by macrophages (0.82 ± 0.07 μM versus 0.96 ± 0.15 μM air versus CO, respectively). CO also had no effect on ATP hydrolysis by ectonucleotidase activity (air plus *E. faecalis*: 213.5 ± 45.41 nmols/min/mg protein versus CO plus *E. faecalis*: 226.61 ± 33.3 nmols/min/mg protein). This implied that ATP was actively produced and released and/or prevented from being metabolized by bacteria. ATP as a DAMP is known to influence NALP3 inflammasome activation. CO exposure of heat-inactivated bacteria showed no increase in ATP levels or IL-1β secretion (data not shown), which suggested to us active release of ATP from bacteria in response to CO. While CO had no effect on bacterial growth (Figure 3E), it did induce a dose-dependent and rapid increase in bacteria-derived ATP versus air-treated controls, as assessed by time-lapse imaging and colorimetric analyses (Figure 5, A and B). The amount of ATP generated by the bacteria in response to CO was similar in magnitude to levels of ATP released from dying cancer cells, which contribute critically to NALP3 inflammasome

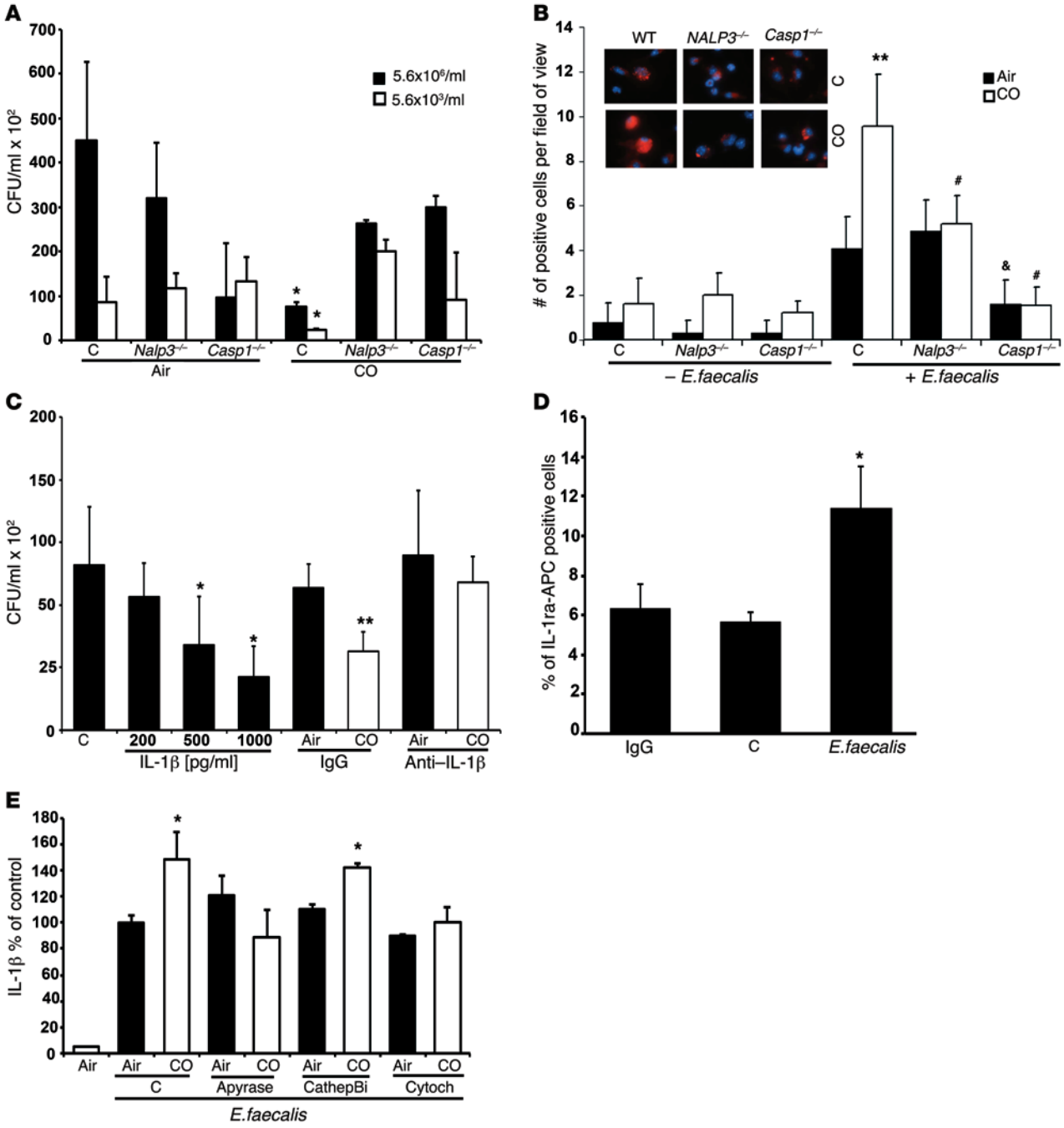

Figure 4. NALP3 is targeted by CO to enhance IL-1β expression and mediate macrophage bacteria killing. (**A**) CFU in WT (air), *Nalp3*$^{-/-}$, and *Casp1*$^{-/-}$ BMDM supernatants infected with *E. faecalis* ± CO. *$P < 0.01$ versus air-treated controls. (**B**) Quantitation and representative images (inset) of cells positive for lysozyme (red) and *E. faecalis* in BMDMs from WT (air), *Casp1*$^{-/-}$, and *Nalp3*$^{-/-}$ mice. Nuclei are stained blue. BMDMs were treated with *E. faecalis* for 1 hour followed by 4 hours of CO (white bars) or air (black bars). **$P < 0.001$, CO versus air; #$P < 0.05$, *Nalp3*$^{-/-}$ versus WT; &$P < 0.05$, *Casp1*$^{-/-}$ versus WT. Original magnification, ×40. (**C**) Bacterial counts in BMDM treated with supernatants ± *E. faecalis* for 1 hour and then treated ± anti–IL-1β or IL-1β recombinant protein. CO (white bars) or air (black bars) was applied as above. *$P < 0.001$, CO versus air; **$P < 0.01$, CO versus air. Results represent mean ± SD of 2 to 4 independent experiments in triplicate. (**D**) Flow cytometry in BMDMs treated with *E. faecalis* for 1 hour or BMDMs with antibody against ILRa-APC. IgG-APC as negative control. Mean ± SD from 3 independent experiments. *$P < 0.05$, *E. faecalis* versus control (C) or IgG. (**E**) IL-1β levels in *E. faecalis*–treated BMDM supernatants as above for 4 hours followed by 1 hour treatment with cathepsin B inhibitor, cytochalasin B, or apyrase. Cells were then exposed to CO or air for 4 hours. Results are presented as percentage of control to account for vehicle effects and represent mean ± SD of 3 independent experiments in duplicate. *$P < 0.05$, comparing CO versus air in both the vehicle-treated control group and the cathepsin B inhibitor-treated group.

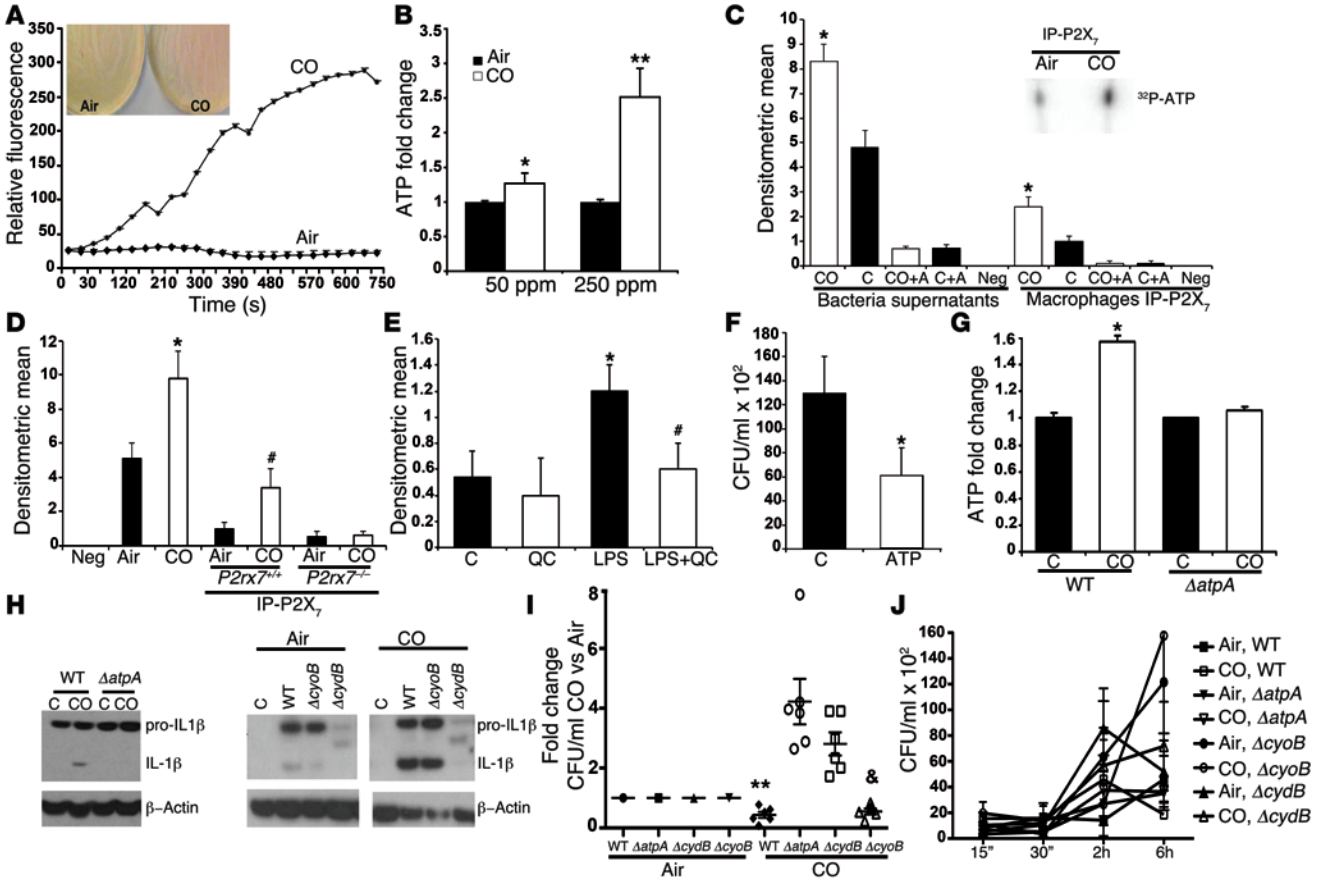

Figure 5. Effects of CO on bacteria-derived ATP generation and macrophage-killing response. (**A**) ATP generation by *E. faecalis* (10^6) ± CO for 1 hour measured colorimetrically (inset) or fluorometrically. (**B**) ATP fluorescence in supernatants from *E. coli* (10^4) treated for 6 hours ± CO. $^*P < 0.05$; $^{**}P < 0.001$. (**C** and **D**) Interaction between *E. coli*–derived ^{32}ATP and immunoprecipitated BMDM P2X$_7$ receptor from WT and *P2rx*$_7^{-/-}$ mice (**D**) treated with supernatant from CO-exposed ^{32}ATP-producing bacteria. Neg, IgG control; A, ampicillin control. $^*P < 0.03$; $^{\#}P < 0.05$, CO versus air. (**E**) ^{32}ATP-producing bacteria supernatant exposed to BMDMs where HO-1 was induced by LPS to increase endogenous CO by HO-1 ± QC-15 to block HO-1. $^*P < 0.01$, LPS versus control (C); $^{\#}P < 0.05$, LPS versus LPS + QC. (**F**) Bacterial counts in BMDM supernatants infected with *E. faecalis* for 1 hour, then ± ATP (50 μM) for an additional 6 hours. $^*P < 0.05$. (**G**) ATP in supernatants of WT *E. coli* MG1665 or ΔatpA *E. coli* (10^4) treated 30 minutes with CO or air expressed as fold change to account for proliferation rate differences. Data represent mean ± SD of 3 experiments in triplicate. $^*P < 0.02$, CO + M1655 versus air + M1655. (**H**) Immunoblot with antibodies against IL-1β lysates of WT or mutant *E. coli*–treated BMDMs ± CO as above. (**I**) Bacterial counts expressed as fold change due to differences in proliferative rates. BMDMs were infected for 1 hour, then treated ± CO for an additional 6 hours. $^{**}P < 0.01$, CO versus WT *E. coli* (10^2). $^*P < 0.05$, CO + ΔcyoB versus air + ΔcyoB; $^{\&}P < 0.04$, CO + Δcyd versus air + Δcyd. (**J**) WT or mutant *E. coli* growth ± CO. Results represent mean ± SD from 3 independent experiments.

activation via a mechanism involving the ATP P2 receptor (53). Important here is that the ATP generated by bacteria was present at concentrations ranging from 3 to 5 μM in CO versus 1 to 2 μM basally and remained elevated and continuously generated by the bacteria when CO was present. This increase in ATP in response to CO likely underestimates the local concentrations at the macrophage cell surface, where ATP is released by the bacteria and likely continues inside the phagosome. We next asked whether bacteria-derived ATP contributed to modulation of macrophage activation by CO. We measured bacterial ATP release and binding to macrophages in response to CO by loading *E. coli* with radiolabeled phosphate (^{32}P) and measuring the amount of ^{32}ATP bound to P2X$_7$ receptors immunoprecipitated from macrophages. A significant increase in ^{32}ATP binding to P2X$_7$ was observed in CO versus air-treated macrophages (Figure 5C). There was no binding of ATP in *P2x*$_7^{-/-}$ macrophages (Figure 5D), suggesting that this is indeed a receptor for ATP originating in the bacteria and then binding to macrophages. To test whether endogenous CO arising from HO-1 exerted the same effects on bacteria, HO-1 was maximally induced in macrophages in response to LPS, and the conditioned medium, when rapidly transferred to ^{32}P-loaded bacteria cultures, showed a significant increase in ^{32}ATP formation (Figure 5E). ^{32}ATP was captured with a bacterial ATP-binding protein, which was subsequently immunoprecipitated and subjected to thin-layer chromatography; the radiolabel was densitometrically quantitated. Importantly, blockade of HO-1 with QC-15 in this scenario completely abrogated the ^{32}ATP increase (Figure 5E). Finally, to demonstrate a functional impact of the elevated ATP, macrophages were treated with exogenous ATP, which recapitulated that observed with CO in enhancing bacterial clearance (Figure 5F). Collectively, these data support a mechanism by which pathogens are recognized and destroyed by the host that involves activation of macrophages by ATP (54, 55).

To further strengthen the concept that bacteria-derived ATP was the DAMP responsible for macrophage activation, we next utilized an *E. coli* strain lacking the ATP synthase subunit A (*ΔatpA*).

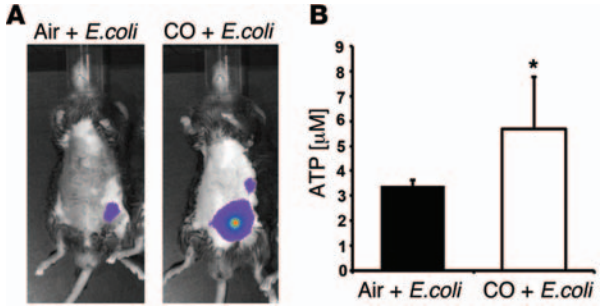

Figure 6. CO increases ATP levels in bacteria-infected mice. (**A** and **B**). ATP measured by IVIS bioluminescence or fluorescence in mouse peritoneal lavages. Mice (n = 4/group) were infected with *E. coli* (10^9) for 1 hour followed by CO for 1 hour. ATP levels were imaged and quantitated 30 minutes after injection of luciferase. *P < 0.05, CO versus air. The stronger signal intensity reflects increased ATP levels evidenced by greater luciferase activity.

This strain survives on alternative, weaker ATP-generating systems. This mutant allowed us to study the molecular target underlying the effect of CO on bacteria-derived ATP. Macrophages were infected with the *ΔatpA E. coli* or with the *E. coli* MG1655 control strain and treated with or without CO. As shown in Figure 5G, unlike what occurred in the MG1655 control strain, CO was unable to increase ATP levels over baseline in the *ΔatpA* mutant, demonstrating that CO promotes production of ATP via a mechanism that in part requires a fully functional ATP synthase. Moreover, macrophages infected with *ΔatpA* in the presence of CO generated very little to no cleaved IL-1β (Figure 5H). We used 2 additional *E. coli* mutants, *ΔcyoB* and *ΔcydB*. These mutants lack the indicated cytochrome oxidase in the bacteria, and it is these heme-containing oxidases that are known to be targets for CO (64). When macrophages were treated with these 2 strains in the presence of CO, we observed an effective increase in IL-1β in the *ΔcyoB* strain that correlated with augmented clearance, but no effect of CO on either IL-1β cleavage or bacteria clearance in the *ΔcydB* strain (Figure 5, H–J). Importantly, both pro and cleaved IL-1β were markedly reduced in *ΔcydB*. From these data, we conclude that CO targets and perhaps binds to heme in the oxidase of *ΔcydB* to compel ATP generation much like that observed in the ATP synthase mutant. Absence of either protein resulted in a loss in CO effects on IL-1β and bacteria killing. While each of the strains exhibited slightly different growth rates, these were not affected by exposure to CO (Figure 5J). Collectively, these data strongly support the notion that bacteria-generated ATP can bind and activate macrophage P2 receptors triggering NALP3/IL-1β/inflammasome–dependent bacterial clearance (57).

CO increases bacteria-derived ATP generation in vivo. The effects of CO on bacterial ATP production were recapitulated in vivo in mice infected i.p. with WT *E. coli*. We took advantage of the fact that luciferase requires ATP to metabolize luciferin and used the luciferase signal intensity as an indirect measure of ATP. Mice exposed to CO showed a significantly enhanced luciferin signal versus air-treated controls, demonstrating the presence of ATP required for luciferase activity (Figure 6, A and B). The luciferin signal was localized to the site of bacteria inoculation in the peritoneal cavity and measured 1 hour after CO, when the amount of bacteria would still be similar between air and CO. These results suggested that the highly diffusible CO accessed the peritoneal cavity and interacted with the bacteria to compel the 2- to 3-fold increase in ATP levels in a manner similar to that generated by bacteria in response to CO in vitro.

CO promotes IL-1β secretion via K^+ channel–dependent activation in macrophages. Given that CO is reported to modulate K^+ channel activity via ATP purinergic receptor signaling (58, 59), we hypothesized that CO modulated NALP3 inflammasome activation through modulation of an ATP-dependent K^+ channel that likely involves one or more P2 receptors (7, 20). First, we measured intracellular K^+ concentrations in macrophages in response to ATP and, as expected, observed a marked decrease in intracellular K^+ levels. Macrophages treated with either bacteria or CO alone had little effect on intracellular K^+ concentrations (Figure 7A). In contrast, macrophages treated with *E. coli* (WT or MG1655) plus CO showed a decrease in intracellular K^+ equivalent to that observed with ATP alone (Figure 7A). Employing the selective K^+ channel inhibitor tetraethylammonium (TEA), we tested the relative contributions of ATP and K^+ channel activity on NALP3 inflammasome activation in response to CO. Mice infected with *E. faecalis* were treated with or without CO and with or without the addition of TEA. PMs were harvested and assessed for caspase-1

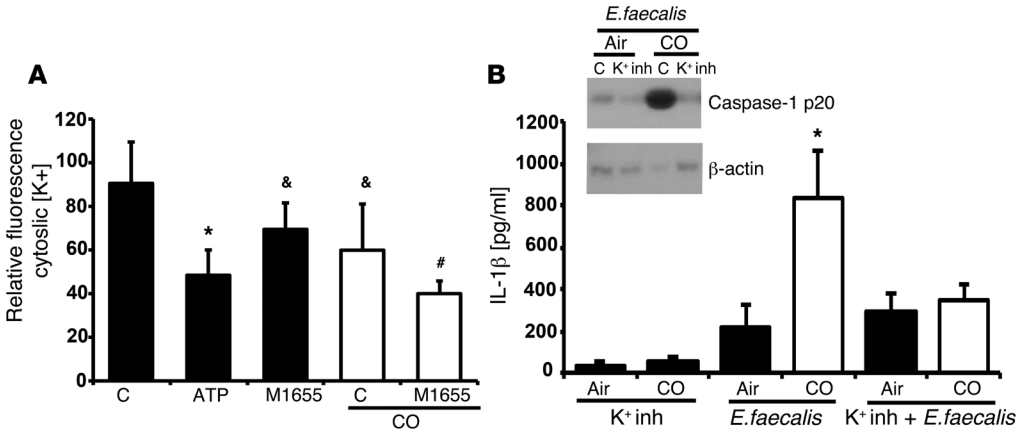

Figure 7. CO modulates potassium flux in vitro and in vivo in macrophages. (**A**) Intracellular potassium (K^+) levels measured fluorometrically in BMDMs infected with *E. coli* (10^4) ± CO. ATP (200 μM) was used as a positive control. Note that both ATP and CO + *E. coli* decreased intracellular K^+ fluorescence, suggesting a K^+ efflux. *P < 0.0001, ATP versus WT; #P < 0.001, M1655+CO versus WT; &P < 0.001, M1655 or CO versus WT. White bars, air; black bars, CO. (**B**) IL-1β ELISA of peritoneal lavage fluid from mice treated ± *E. faecalis* (10^6) ± K^+ channel inhibition with TEA ± CO. CO was started 1 hour after infection and continued for 1 hour. *P < 0.01 CO versus control (C). All results represent mean ± SD of 2 to 4 independent experiments with n = 3–6/group.

cleavage and IL-1β expression. TEA suppressed the ability of CO to increase caspase-1 activation and IL-1β secretion compared with controls linking K^+ channel to inflammasome activity. (Figure 7B). The inability of TEA to block IL-1β expression to levels below that observed with *E. faecalis* alone suggests other ATP-dependent, non–K^+ channel–mediated mechanisms involved in the activation of IL-1β, such as P2Y receptors (57). Collectively, these findings speak to the selectivity of CO in modulating IL-1β via P2 receptor signaling, perhaps suggesting differences in ATP affinity for each purinergic receptor.

CO protects against sepsis-induced multiorgan failure in mice. To test our in vitro observations in a clinically relevant experimental model of bacterial infection in vivo, we inoculated mice i.p. with a lethal dose of *E. faecalis* prior to therapeutic administration of inhaled CO. Caspase-1 cleavage and IL-1β secretion were measured in peritoneal exudates. We observed a significant time-dependent induction of IL-1β cleavage/secretion in PMs in response to bacteria, an effect enhanced by inhaled CO (Figure 8, A–C). Of note, IL-1β cleavage/secretion was measured in total peritoneal exudates, which likely involves cell types other than macrophages. While the effects of CO on IL-1β expression and corresponding caspase-1 cleavage were evident in peritoneal leukocytes, this was not associated with a systemic increase in IL-1β, suggesting that CO acts at the primary site of infection targeting live bacteria, compelling their release of ATP, which in turn drives increased IL-1β secretion by activated macrophages. Moreover, CO also promoted more rapid resolution of inflammation, as suggested by the more rapid decrease in IL-1β expression, which occurred as early as 4 hours after infection compared with that of controls treated with air at the same time point. The more rapid resolution of the infection correlated with a greater than 50% increase in bacterial clearance over controls as well as improved survival and inhibition of multiorgan failure (Figure 8). CO protected against sepsis-induced gut epithelial cell sloughing in the colon and acute liver injury as assessed by reduced levels of serum transaminases (ALT) (Figure 8, D and E). Acute kidney injury was also abrogated. Elevated serum blood urea nitrogen (BUN) levels as a measure of kidney damage were lower in CO-treated mice compared with air-treated controls (97.3 ± 16.3 mg/dl in air versus 32.0 ± 19.4 in CO-treated mice, $P < 0.02$; normal BUN = 18–29 mg/dl). Real-time IVIS imaging using chemiluminescent *E. coli* (Xen 14) corroborated the ability of CO to augment bacterial clearance (Figure 8F). Leukocyte infiltration into the peritoneal cavity in response to bacterial administration showed an increase in neutrophils (PMN) at 4 hours after infection ($10.4 \pm 1.1 \times 10^6$ versus $1.3 \pm -0.3 \times 10^6$ in untreated controls $P < 0.02$). PMN cell infiltration was modestly reduced in CO-treated mice ($6.1 \pm 1.9 \times 10^6$) over the same time interval, correlating with the decreased bacterial counts and modulation of the inflammatory response (Figure 8, A and F).

Mice infected i.p. with *E. faecalis* and exposed to air succumbed to lethal septic shock (75% mortality) within 24 to 48 hours (Figure 8G). Inhaled CO, when initiated 1 hour after infection, resulted in 100% survival, while exposure to CO initiated as long as 6 hours after bacterial injection resulted in 60% survival (Figure 8G). The experiments were stopped at 4 days, which was considered long-term survival. CO also conferred protection in a cecal ligation and puncture (CLP) model of sepsis. CO administered 1 hour after CLP increased survival to 60% compared with 5% in air-treated controls (Figure 8G).

CO requires NALP3 and caspase-1 to impart protective effects against lethal infection and is able to rescue mice deficient in HO-1. Our in vitro evidence supporting a role for the NALP3 inflammasome on the CO effects led us to next inoculate *Nalp3*$^{-/-}$ and *Casp1*$^{-/-}$ mice with *E. faecalis* and measure clearance. Mice deficient in either protein were unresponsive to CO in the lethal sepsis model or bacterial killing assay, and *Casp1*$^{-/-}$ mice showed a significant deficit in the ability to kill bacteria with or without CO present (Figure 8, H and I). These data suggest that CO requires activation of caspase-1 and the resulting IL-1β release to promote bacterial clearance, confirming our in vitro observations (Figure 4).

Animals lacking HO-1 activity are exquisitely sensitive to bacterial infection (32, 37). Importantly, CO was able to rescue a significant percentage of inoculated *LyzM-Cre Hmox1*$^{fl/fl}$ mice (HO-1 absent in myeloid cells) and WT mice in which HO activity was inhibited with Sn-PP-IX (Figure 8, J and K).

Discussion

Pathogen recognition by germline-encoded PRR is a paramount requirement for host protection against infection (60, 61). However, PRR do not sense the metabolic activity status of the pathogen recognized and hence evaluate its potential pathogenicity. Pathogen detection and elimination must be metabolically efficient, highly specific, and complete, with indispensable secondary and perhaps tertiary regulatory checkpoints. We propose that when generated endogenously by HO-1, CO is deployed by the host to reveal the presence of metabolically functional bacteria, revealed by the generation of bacterial ATP, which amplifies the macrophages' killing machinery. Moreover, we demonstrate that under physiologic conditions, CO is required for appropriate activation of the NALP3 inflammasome, leading to caspase-1 activation via selective triggering of a K^+ channel by bacterial ATP, which results ultimately in secretion of IL-1β, bacterial phagocytosis, and killing. These effects are likely not related to decreased oxygen availability because similar immunomodulatory effects on macrophage activation were not observed under hypoxic conditions (25). Paradoxically, CO improves oxygenation during ischemic stress (62).

Under homeostatic conditions, HO-1 is expressed mainly in hematophagocytic macrophages in the red pulp of the spleen, being strongly induced in all other tissue-resident macrophages once these sense the presence of bacteria and other stress-related conditions (29). Presumably, this allows HO-1 to confer a natural mechanism for innate immune cell regulation in the context of bacterial recognition. In keeping with this notion, HO-1 deletion increases sensitivity to bacterial infection, an effect associated with a marked deficit in the ability of the macrophages to evoke an archetypical bacterial clearance response. As demonstrated herein, this impairment in the macrophage response is driven by defective IL-1 processing via the NALP3 inflammasome/caspase-1 pathway, revealing an unsuspected mechanism by which macrophages using the HO-1/CO system sense the metabolic status of pathogens, namely, their capacity to produce ATP in response to this highly diffusible gas. This would then allow the macrophages to modu-

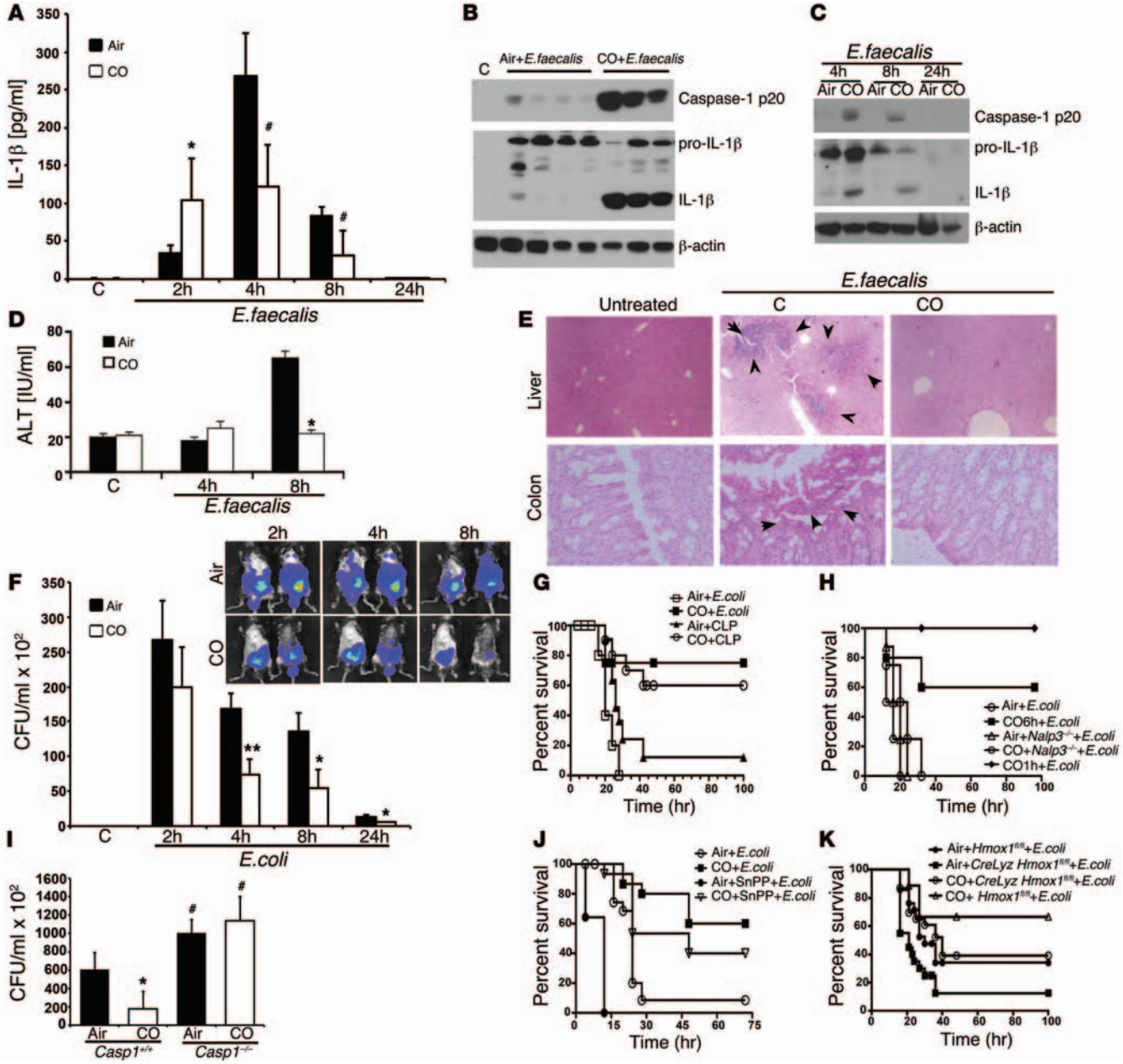

Figure 8. CO acts therapeutically to inhibit lethal sepsis via the inflammasome. (**A**) IL-1β in peritoneum from mice infected with *E. faecalis* (10^9 CFU) for 1 hour ± CO. Data represent mean ± SD of $n = 6$/group in triplicate. $^*P < 0.01$; $^\#P < 0.05$, CO versus air. (**B**) Immunoblot of cleaved caspase-1 and IL-1β in PM lysates from mice infected with *E. faecalis* for 1 hour prior to 1 hour treatment with air or CO. Representative blot from 3 independent experiments. (**C**) Immunoblots of macrophages lysates from mice treated as in **B**. (**D**) ALT in infected mice treated as above. Results represent mean ± SD ($n = 4$–6/group) from 3 experiments. $^*P < 0.001$, CO versus air. (**E**) H&E staining 8 hours after *E. faecalis* ± CO; 6 to 10 images per animal. Arrows indicate lesions. Original magnification, ×20. (**F**) Bacterial counts in peritoneal lavagates. Inset: IVIS images. Results represent mean ± SD of 6 to 8/group. $^*P < 0.05$; $^{**}P < 0.01$. (**G**) Survival in mice injected with lethal *E. coli* (10^{10} CFU, i.p.) or CLP ± 4 hours CO initiated 6 hours later. $P < 0.02$, air + CLP versus CO + CLP; $P < 0.02$, air + *E. coli* versus CO + *E. coli*. (**H**) Survival of WT and *Nalp3*$^{-/-}$ mice treated as in **G** with or without CO (started 1 or 6 hours after bacteria). CO was unable to protect *Nalp3*$^{-/-}$ mice ($P < 0.01$). (**I**) Bacteria counts in peritoneum of *E. coli*–infected mice. Results represent mean ± SD of 4 to 6/group repeated twice. $^*P < 0.03$, CO versus air; $^\#P < 0.05$, *Casp1*$^{-/-}$ versus *Casp1*$^{+/+}$ in both air and CO-treated mice. (**J**) Survival ± Sn-PP-IX to block HO-1 then ± 4 hours CO beginning 1 hour after bacteria. $P < 0.05$, 10/group. (**K**) Survival of indicated mice ± CO as in **G**. $P < 0.03$. $n = 10$–30/group.

late activation of the NALP3 inflammasome/caspase-1 pathway, achieving pathogen clearance while limiting tissue damage.

CO binds to heme-containing bacterial respiratory complexes located on the outer membrane to produce ATP, leading to inflammasome activation and ultimately bacterial clearance. While ATP was thought to arise from intracellular stores following host cell death (63), we now describe how CO compels bacteria to generate this second signal, which permits more efficient elimination versus direct bacterial lysis. In the absence of bacterial ATP, the local inflammation elicited by metabolically inactive bacteria or endotoxin is resolved without instigation of a nonspecific immune response.

Spectral analyses of the *E. coli* cytochrome complex showed that CO binds to the heme component of the bacterial subunit 1 oxidase, which is involved in aerobic oxidative respiration and contributes to the generation of ATP (64). The cydB terminal oxidase, which preferentially functions as a proton motive force under anaerobic conditions, when absent in the *ΔcydB* bacteria, abrogated the ability of CO to regulate IL-1β and bacterial clearance. Indeed, basal expression of pro–IL-1β was strikingly reduced in the cydB mutant and markedly amplified in the *ΔcyoB* knockout, where cydB oxidase was likely overexpressed in compensating for the absence of cyoB. In addition to the necessary proton motive force, interfering with the ATP synthase, which lies further downstream of the oxidases toward the generation of ATP, also negated the effects of CO on bacterial clearance and IL-1β expression (Figure 5). It is well established that ATP acts through macrophage purinergic receptors (both P2X and P2Y) to achieve NALP3 inflammasome activation (7, 57). A significantly reduced inflammasome response leads to inefficient release of IL-1β, compromising bacterial clearance, which we demonstrate can be rescued in macrophages with addition of recombinant IL-1β (Figure 4). This paradigm may reflect expression of IL-1β, which functions to enhance macrophage activation. This enhanced activation has been reported to influence the phagocytic and/or metabolic state of the macrophage (65). Hedl and Abraham demonstrated that IL-1β can auto activate MAP kinases and NOD2 responses in macrophages (63). We find that IL-1β neutralization affects the killing capabilities of the macrophages. Indeed, work by Kanangat et al. suggests that low doses of IL-1β (up to 250 pg/ml) inhibit bacterial growth while higher levels of IL-1β promote growth (66).

We found a unique metabolic interaction between host and microbe and put forth an efficient 2-hit system for the recognition by innate immune cells of metabolically active microbes, presumably acting as the earliest immune response against pathogen invasion. Were only one signal required, host macrophages would likely exist in an ongoing unfettered activation state, particularly in the peritoneum, gastrointestinal tract, and the liver, where intestinal endotoxin levels fluctuate with intestinal microbes in close proximity. In such instances, mounting a full inflammatory response would be metabolically costly, inefficient, and potentially detrimental to the organism.

Our observations are applicable to Gram-positive and -negative bacteria as well as *Mycobacterium bovis* bacillus Calmette-Guérin (Mtb-BCG), but interestingly, were not apparent in response to *S. typhimurium*. Perhaps this is explained in part by alternative kinetics of the response or by the fact that *Salmonella*, being primarily intracellular, results in activation of alternative macrophage clearance pathways directed by an intracellular CO-ATP axis and dependent on NLRC4 (67). HO-1 is also localized and active in high levels intracellularly in the endoplasmic reticulum and mitochondria.

In summary, we unveil a unique and evolutionarily conserved paradigm for innate sensing of metabolically active microbes in which CO, deployed from innate immune cells, acts on behalf of the host and serves as a metabolic scout for the presence of live bacteria. Should it confront viable, pathogenic bacteria, CO binds to its respiratory heme complexes, inducing the release of ATP, a danger signal that activates a lytic response in innate immune cells. Collectively, we describe a compelling model (Figure 9) by which the macrophage and microbe communicate in a way that ensures host survival (Figure 9). When acting in the context of PRR ligation, CO participates in the efficient marking of pathogens, unleashing a cytotoxic response aimed at pathogen clearance.

Methods

Bacteria isolation and propagation

E. coli (DH5α strain, ATCC), *E. coli Xen 14* (chemiluminescent *EPEC WS2572*–parental strain, Caliper Life Sciences), *Salmonella enterica* (*S. typhimurium*) (ATCC), Mtb-BCG (provided by William Bishai, Johns Hopkins University, Baltimore, Maryland, USA), and *E. faecalis* or *E. coli* (single colony isolated from mouse intestinal flora) were used. Additionally, *E. coli MG1655* and knockout strains (*ΔatpA*, *ΔcydB*, *ΔcyoB*) originally acquired from the Keio library were provided by Bernard Strauss (Massachusetts Institute of Technology [MIT], Cambridge, Massachusetts, USA). A single colony of each type of bacteria was isolated from the agar plate and cultured overnight in an orbital shaker in LB medium (*E. coli*, *E. faecalis*), nutrient broth (*S. typhimurium*), or in Lowenstein Jensen Medium with Mycobacterial Supplement (*M. bovis*, Sigma-Aldrich). After determination of an initial absorbance at 600 nm, dilutions were prepared in antibiotic-free medium to permit using macrophages at indicated doses. Samples of dilutions were dilution plated to determine CFU (CFU/ml). For in vitro experiments, the amount of bacteria averaged 10^6 CFU/ml (MOI of 40–50) for *E. faecalis* and 10^4 CFU/ml (MOI of 1–10) for *E. coli* unless otherwise indicated. For infection in vitro, no antibiotics were used unless indicated and macrophages were washed twice with PBS prior to infection to remove any residual antibiotics. We performed pilot dose escalation experiments using *E. faecalis* and *E. coli* and found that doses of 10^4 and 10^6 CFU/ml of *E. coli* and *E. faecalis*, respectively, did not induce macrophage death at up to 10 hours (crystal violet exclusion, data not shown) and stimulated pro–IL-1β cleavage (Figure 1); the bacteria were killed by macrophages (Figure 3. Higher doses of bacteria killed macrophages by 10 hours. Therefore, in our in vitro studies, we used either 10^6 or 10^4 CFU/ml of *E. faecalis* and *E. coli*, respectively. Under these conditions, induction of pro–IL-1β occurs at between 4 and 6 hours. These amounts of bacteria in culture correlated with an overwhelming infection in the animal models.

Cell culture

BMDMs from mice were harvested and differentiated as previously described (68). For each experiment, cells were seeded at a density of 1 to 2 million per 60 mm plate. PMs were isolated by washing peritoneum of mice with 1 ml, 1× PBS. Cells were then centrifuged and resus-

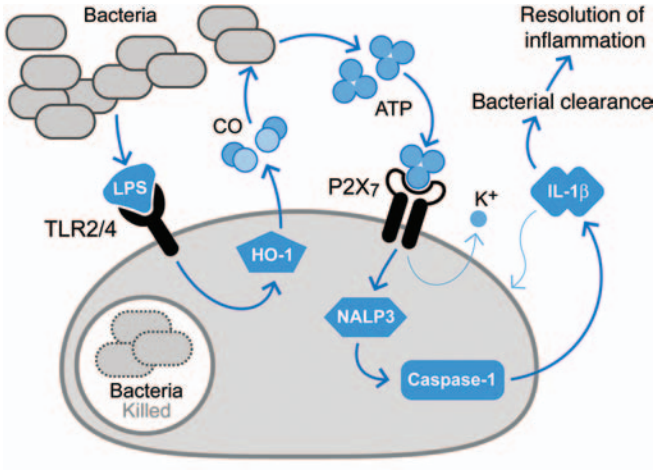

Figure 9. Schematic depicting a proposed mechanism of action for HO-1 and CO in bacteria recognition and activation of innate immune defense machinery. As a highly diffusible gas, HO-1 is induced by endotoxin (LPS) from bacteria and generates CO. CO is emitted by the host macrophage and functions to probe and "assess" the environment. If bacteria are present, CO compels the bacteria to generate ATP, which acts as a danger signal for the macrophage. The bacteria-derived ATP binds to a purinergic receptor on the macrophage, leading to changes in intracellular K^+ concentrations. This signal in turn activates the inflammasome to drive pathogen clearance.

pended in RPMI medium (Life Technologies) with 10% FBS (Atlanta Biologicals). PMs were used for experiments after 24 hours of culture in vitro. In all experiments, BMDMs or PMs were challenged with the indicated bacterium ± CO (250 parts per million [ppm]) or air as described previously (69).

Retroviral transduction of BMDMs with shRNA. BM cells were isolated and cultured in the medium containing SCF (100 ng/ml), IL-6 (10 ng/ml), and IL-3 (6 ng/ml) (PeproTech) for 24 hours. Retroviral microadapted shRNA was prepared as described (68). Cells were transduced 12 hours with retroviruses in medium containing Polybrene (8 μg/ml, Sigma-Aldrich). Twenty-four hours later, MCSF (Peprotech) was added for differentiation into macrophages as above.

Reagents

TEA (Calbiochem; Millipore), a nonspecific BK channel inhibitor, was dissolved in water. Mice were treated with TEA (30 mg/kg, i.p.) 30 minutes before treatment with CO or air. In vitro TEA (1 μM), NAC (20 mM), cathepsin B inhibitor (10 μM), apyrase (5 U/ml), cytochalasin B, (5 μg/ml), and LPS (10 ng/ml) were purchased from Sigma-Aldrich. QC-15 (25 μM) was provided by D. Nakatsu (Queen's University, Kingston, Ontario, Canada). Sn-PP-IX (30 μM), and biliverdin (50 μM) were purchased from Frontier Scientific. Recombinant IL-1β (200–1000 pg/ml, R&D Systems) or ATP (50 μM) was applied 1 hour before CO treatment. Anti-mouse neutralizing IL-1β/IL-1F2 Abs (100 ng/ml, R&D Systems) were applied 15 minutes prior to CO treatment.

Phagolysosome staining. BMDMs were treated with bacteria as described above for 1 hour, and CO or air was then applied for 4 hours. For the last 30 minutes of treatment, cells were loaded with LysoTracker Red DND-99 (Molecular Probes; Invitrogen). Hoechst staining (Molecular Probes; Invitrogen) was applied on 2% PFA-fixed cells. Pictures were taken under ×40 magnification on a Zeiss Apotome Axiovert Fluorescence Microscope.

Animals

Nalp3$^{-/-}$, *Casp1*$^{-/-}$, and control WT animals were generated as previously described (23). C57BL/6 mice as well as type 1 *Il1r*$^{-/-}$, *Tlr4*$^{-/-}$, and *LyzM*-Cre recombinase animals were purchased from Jackson Laboratories. *Tlr2*$^{-/-}$ mice were provided by Hong Jun Wang (BIDMC). *Hmox1*$^{-/-}$ mice were generated as previously described (3). *Hmox1*$^{fl/fl}$ mice were provided by the RIKEN BRC through the National Bio-Resource Project, Japan. The characterization of these mice was previously reported (4). *Hmox1*$^{fl/fl}$ mice were bred with *LyzM-Cre* mice(Jackson Laboratories), and *LyzM-Cre Hmox1*$^{fl/fl}$ homozygotes were identified by genotyping (70). In all experiments, animals were treated with bacteria for 1 to 6 hours at the indicated concentrations in a volume of 500 μl i.p. prior to being exposed to CO (250 ppm). The amounts of bacteria were selected from a combination of preliminary dose-ranging studies and literature review (32, 71, 72). The amount of bacteria administered ranged from 10^4 to 10^{10}, depending on whether the studies were sublethal or lethal in design, to assess relevant readouts associated with the pathophysiology of sepsis. Doses are listed in Methods and figure legends. Sn-PP-IX or saline vehicle as control was used at 50 mg/kg 16 and 5 hours prior to bacterial infection.

CLP. Male C57BL/6 mice (Jackson Laboratories) were at ages 6 to 8 weeks and weighed 20 to 25 g. Briefly, animals were anesthetized with pentobarbital (70 mg/kg, i.p.); a 1- to 2-centimeter midline laparotomy was performed and the cecum identified. Stool was then milked to the tip of the cecum and ligated 1 centimeter from the tip with 2-0 silk. The cecum was then perforated with a 22-gauge needle and returned to the abdomen. The musculature and skin were closed with a running 2-0 silk suture. Sham animals underwent laparotomy and bowel manipulation without ligation or perforation.

Histopathology. Liver and small intestine were harvested, fixed in 10% paraformaldehyde, and stained with H&E. Images were captured as previously described (28, 35).

ATP measurement

ATP in samples was determined colorimetrically and fluorometrically using commercial assay kits (BioVision Inc). Macrophages were inoculated with bacteria for 4 hours, followed by treatment with CO or air. Supernatants were cleared by centrifugation at 500 *g* for 5 minutes prior to analyses. In similar experiments, bacteria were viewed with a Zeiss Axiovert Apotome Microscope and fluorescence measured in real time in the presence of air or CO (250 ppm). For colorimetric determination of ATP, 0.5 ml of reaction mix was directly applied to the bacteria-coated plates. Plates were treated with or without CO for 1 hour, and the development of color (pink) indicated ATP production.

IVIS. In vivo imaging of ATP production was measured in the Longwood Medical Small Animal Imaging Facility (SAIF), BIDMC, indirectly using luciferase (Sigma-Aldrich). ATP generation in response to *E. coli* infection was measured in the peritoneum with or without CO after injection of equal amounts of D-luciferin and luciferase (20 mg/kg each i.p., Sigma-Aldrich). The intensity of bioluminescence corresponded indirectly to ATP levels. ATP is required for luciferase activity, and thus an increase in luciferase signal reflects in part the available ATP. ATP was also determined in cell-free peritoneal lavagates using the fluorescent assay kit as described above.

^{32}ATP interaction with P2X$_7$ and bacterial ATP-binding protein. *E. coli* were cultured in phosphate-free medium supplemented with 0.2 mCi ^{32}P for 2 hours. As a control, a separate culture of bacteria

was treated with ampicillin. Bacterial cultures were washed twice with PBS and subjected to centrifugation at 2,500 *g* for 10 minutes to pellet bacteria to remove nonincorporated ^{32}P. *E. coli* were then treated with the ENT inhibitor POM-1 and exposed to CO for 15 minutes. Cultures were collected, and bacteria were pelleted. The supernatant was collected and then added to macrophage cultures for 3 minutes. Cells were washed with PBS and then lysed in 250 μl buffer A (20 μM Tris with 100 μM phenylmethylsulfonylfluoride, 1 μM leupeptin, 1 μM sodium orthovanadate, 10 mM $MgCl_2$, and 1% Triton X-100) for 15 minutes. Nuclei were pelleted by centrifuging at 10,000 *g* for 10 minutes. For the experiments with endogenous HO-1–derived CO, BMDMs were treated with LPS (10 ng/ml) to induce HO-1 and then treated with or without QC-15 (25 μM). The supernatants from these cells were then rapidly transferred onto bacteria as described above. The supernatants were incubated with His-tagged rbsA recombinant protein (MBS1123212; MyBioSource) for 30 minutes at 37°C.

BMDMs or bacterial lysates from the above were immunoprecipitated with anti-$P2X_7$ or anti-His antibody, and the immunoprecipitate was subjected to thin-layer chromatography (polyethyleneimine cellulose on polyester from Sigma-Aldrich) by using 0.75 M KH_2PO_4. Intensity of ATP was determined by phosphor imaging. Data are presented as intensity as a percentage of the macrophage cultures treated with the supernatant from ^{32}P-treated bacteria treated in standard culture (without CO) or as a fold change from bacteria cultures treated with the supernatant from BMDMs treated with LPS and no HO-1 inhibitor (QC-15).

Potassium flux

FluxORTM Potassium Ion Channel Assay (Life Technologies) was used to measure the cytosolic levels of K^+. BMDMs were seeded in 6-well plates and infected with *E. coli* for 4 hours, followed by incubation for 1 hours at 24°C with loading buffer following the manufacturer's protocol. Cells were treated with CO or ATP for 30 minutes and scraped from the plates immediately after treatment. Basal fluorescence was recorded in 96-well plates in the cell suspensions using FITC filters. Stimulus buffer was added, and the fluorescence corresponding to the cytosolic levels of K^+ was measured within 5 minutes.

Bacterial killing in vivo and in vitro

Samples for bacterial count determination were diluted from ×10 to 1,000×, and 20 μl were plated on LB-agar plates and incubated overnight in triplicate; the dilution that gave a minimal count of 200 colonies/plate was used to determine clearance as previously described (37). Initial doses and kinetics are presented in the figure legends.

Bioluminescence. Bacteria counts in vivo were also measured by employing the bioluminescent *E. coli* strain *Xen 14*. Mice were injected with *Xen 14*, followed 1 hour later by CO (250 ppm) or air exposure for 1 hour. Bioluminescence was measured over time in anesthetized animals (2% v/v isoflurane) at specified intervals using a Xenogen IVIS–50 Bioluminescence Reader housed and operated by the BIDMC Small Animal Imaging Facility. Luciferase or D-Luciferin was injected where indicated (20 mg/kg, i.p.), and imaging commenced immediately.

ALT measurement

Whole-blood samples were centrifuged at 6,000 *g* for 5 minutes, and the serum was collected. Aminotransferase levels were measured using Automated Diagnostic Analyzer (IDEXX Laboratories).

ELISA

Mouse IL-1β and TNF-α ELISA (R&D Systems) were performed in cell culture supernatants, serum, or peritoneal washes following the manufacturer's protocol.

RNA isolation, cDNA synthesis, and real-time PCR

RNA was isolated from cell lysates following the manufacturer's protocol using RNeasy Mini RNA Isolation Kit (QIAGEN). cDNA was synthesized using 2 μg RNA and transcribed with the cDNA Synthesis Kit (BioRad). Real-time PCR was performed with SYBR Green PCR Master Mix (BioRad) and the following primers: IL-1β, forward: 5′-TGGGCCTCAAAGGAAAGA-3′, reverse: 5′-GGTGCTGATGTACCAGTT-3′; ASC, forward: 5′-AGACATGGCTTACAGGA-3′, reverse: 5′-CTCCTCATCTTGTCTTGG-3′; HO-1, forward: 5′-CAGGATTTGTCAGAGGCCCTGAAGG-3′, reverse: 5′-TGTGGTACAGGGAGGCCATCACC-3′; actin, forward: 5′-TAGACTTCGAGCAGGAGATGGC-3′, reverse: 5′-CCACAGGATTCCATACCCAAGA-3′; caspase-1, forward: 5′-TGAAAGAGGTGAAAGAATT-3′, reverse: 5′-TCTCCAAGACACATTATCT-3′; NLRP3/NALP3, forward: 5′-CTGTGTGTGGGACTGAAGCAC-3′, reverse: 5′-GCAGCCCTGCTGTTTCAGCAC-3′; and P2X7, forward: 5′-CGAGTTGGTGCCAGTGTGGA-3′, reverse: 5′-CCTGCTGTTGGTGGCCTCTT-3′. HO-1 primers were previously described (2).

Immunoblotting

Immunoblotting was performed as previously described (42). β-Actin (Sigma-Aldrich), pro–IL-1β (Milipore), caspase p20 (Cell Signaling), and IL-1β antibody (Millipore) were acquired as indicated. HO-1 antibodies were from Calbiochem/Millipore or Epitomics/Abcam. Total Akt antibody was purchased from Cell Signaling.

Statistics

All values are expressed as the average ± SD. All experiments were repeated as at least 2 to 3 independent experiments in duplicate or triplicate. Samples were analyzed using 1-way ANOVA followed by Tukey's multiple comparison test or Student's *t* test (2 tailed). A *P* value of less than 0.05 was considered to be significant. When appropriate, Kruskal Wallis and Mann-Whitney tests were applied. Analyses were performed using SPPS13.0 and/or Graphpad; consultation was with Shiva Gautam, biostatistician at the Harvard University Clinical and Translational Science Center.

Study approval

Animal protocols were approved by the Institutional Animal Care and Use Committees at the BIDMC, the Gulbenkian Institute, Yale University, Alfama Inc., and the University of Pittsburgh Medical Center.

Acknowledgments

This work was largely supported by NIH grants HL-071797 and HL-076167 (to L.E. Otterbein) and American Heart Association grants 10SDG2640091 and NIH R21CA169904-01 (to B. Wegiel). We thank Bryan Davis (MIT/Harvard Medical School) and Bernard Strauss (MIT) for providing mutant strains from the Keio *E. coli* knockout library. We are grateful to D. Nakatsu for providing QC-15. We thank the Julie Henry Fund at the Transplant Center of the

BIDMC for their support. L.E. Otterbein holds an honorary visiting professorship at Aston University (Birmingham, United Kingdom). This work was supported by Fundação para a Ciência e Tecnologia (Portugal) grants SFRH/BPD/25436/2005 and PTDC/BIO/70815/2006 (to R. Larsen) and PTDC/BIA-BCM/101311/2008 and PTDC/SAU-FCF/100762/2008 (to M.P. Soares), the European Community, 6th Framework grant LSH-2005-1.2.5-1 and ERC-2011-AdG, 294709 – DAMAGECONTROL (to M.P. Soares), and in part by NIH grant HL-106227 (to E. Kaczmarek). R. Flavell is an investigator of the Howard Hughes Medical Institute.

Address correspondence to: Leo E. Otterbein, Harvard Medical School, Beth Israel Deaconess Medical Center, Transplant Institute, Center for Life Sciences, 3 Blackfan Circle, Boston, Massachusetts 02215, USA. Phone: 617.735.2851; E-mail: lotterbe@bidmc.harvard.edu.

1. Medzhitov R, Janeway C, Janeway C Jr. Innate immune recognition: mechanisms and pathways. *Immunol Rev*. 2000;173:89–97.
2. Medzhitov R, Janeway C, Janeway C Jr. Innate immunity. *N Engl J Med*. 2000;343(5):338–344.
3. Sutterwala FS, Ogura Y, Flavell RA. The inflammasome in pathogen recognition and inflammation. *J Leukoc Biol*. 2007;82(2):259–264.
4. Sutterwala FS, et al. Critical role for NALP3/CIAS1/Cryopyrin in innate and adaptive immunity through its regulation of caspase-1. *Immunity*. 2006;24(3):317–327.
5. Tschopp J, Schroder K. NLRP3 inflammasome activation: The convergence of multiple signalling pathways on ROS production? *Nat Rev Immunol*. 2010;10(3):210–215.
6. Agostini L, Martinon F, Burns K, McDermott MF, Hawkins PN, Tschopp J. NALP3 forms an IL-1β-processing inflammasome with increased activity in Muckle-Wells autoinflammatory disorder. *Immunity*. 2004;20(3):319–325.
7. Mariathasan S, et al. Cryopyrin activates the inflammasome in response to toxins and ATP. *Nature*. 2006;440(7081):228–232.
8. Martinon F, Burns K, Tschopp J. The inflammasome: a molecular platform triggering activation of inflammatory caspases and processing of proIL-β. *Mol Cell*. 2002;10(2):417–426.
9. Ogura Y, Sutterwala FS, Flavell RA. The inflammasome: first line of the immune response to cell stress. *Cell*. 2006;126(4):659–662.
10. Sutterwala FS, Ogura Y, Zamboni DS, Roy CR, Flavell RA. NALP3: a key player in caspase-1 activation. *J Endotoxin Res*. 2006;12(4):251–256.
11. Lara-Tejero M, et al. Role of the caspase-1 inflammasome in Salmonella typhimurium pathogenesis. *J Exp Med*. 2006;203(6):1407–1412.
12. Sutterwala FS, Mijares LA, Li L, Ogura Y, Kazmierczak BI, Flavell RA. Immune recognition of Pseudomonas aeruginosa mediated by the IPAF/NLRC4 inflammasome. *J Exp Med*. 2007;204(13):3235–3245.
13. Petrilli V, Dostert C, Muruve DA, Tschopp J. The inflammasome: a danger sensing complex triggering innate immunity. *Curr Opin Immunol*. 2007;19(6):615–622.
14. Williams JH, Ireland HE. Sensing danger—Hsp72 and HMGB1 as candidate signals. *J Leukoc Biol*. 2008;83(3):489–492.
15. Martin-Murphy BV, Holt MP, Ju C. The role of damage associated molecular pattern molecules in acetaminophen-induced liver injury in mice. *Toxicol Lett*. 2010;192(3):387–394.
16. Scheibner KA, Lutz MA, Boodoo S, Fenton MJ, Powell JD, Horton MR. Hyaluronan fragments act as an endogenous danger signal by engaging TLR2. *J Immunol*. 2006;177(2):1272–1281.
17. Martinon F, Petrilli V, Mayor A, Tardivel A, Tschopp J. Gout-associated uric acid crystals activate the NALP3 inflammasome. *Nature*. 2006;440(7081):237–241.
18. Hornung V, et al. AIM2 recognizes cytosolic dsDNA and forms a caspase-1-activating inflammasome with ASC. *Nature*. 2009;458(7237):514–518.
19. Joshi VD, Kalvakolanu DV, Hebel JR, Hasday JD, Cross AS. Role of caspase 1 in murine antibacterial host defenses and lethal endotoxemia. *Infect Immun*. 2002;70(12):6896–6903.
20. Petrilli V, Papin S, Dostert C, Mayor A, Martinon F, Tschopp J. Activation of the NALP3 inflammasome is triggered by low intracellular potassium concentration. *Cell Death Differ*. 2007;14(9):1583–1589.
21. Fritz JH, Ferrero RL, Philpott DJ, Girardin SE. Nod-like proteins in immunity, inflammation and disease. *Nat Immunol*. 2006;7(12):1250–1257.
22. Grahames CB, Michel AD, Chessell IP, Humphrey PP. Pharmacological characterization of ATP- and LPS-induced IL-1beta release in human monocytes. *Br J Pharmacol*. 1999;127(8):1915–1921.
23. Eisenbarth SC, Colegio OR, O'Connor W, Sutterwala FS, Flavell RA. Crucial role for the Nalp3 inflammasome in the immunostimulatory properties of aluminium adjuvants. *Nature*. 2008;453(7198):1122–1126.
24. Piccini A, Carta S, Tassi S, Lasiglie D, Fossati G, Rubartelli A. ATP is released by monocytes stimulated with pathogen-sensing receptor ligands and induces IL-1β and IL-18 secretion in an autocrine way. *Proc Natl Acad Sci U S A*. 2008;105(23):8067–8072.
25. Otterbein LE, et al. Carbon monoxide has anti-inflammatory effects involving the mitogen-activated protein kinase pathway. *Nat Med*. 2000;6(4):422–428.
26. Vile GF, Basu-Modak S, Waltner C, Tyrrell RM. Heme oxygenase 1 mediates an adaptive response to oxidative stress in human skin fibroblasts. *Proc Natl Acad Sci U S A*. 1994;91(7):2607–2610.
27. Lee PJ, Alam J, Wiegand GW, Choi AM. Overexpression of heme oxygenase-1 in human pulmonary epithelial cells results in cell growth arrest and increased resistance to hyperoxia. *Proc Natl Acad Sci U S A*. 1996;93(19):10393–10398.
28. Soares MP, et al. Expression of heme oxygenase-1 can determine cardiac xenograft survival. *Nat Med*. 1998;4(9):1073–1077.
29. Otterbein LE, Soares MP, Yamashita K, Bach FH. Heme oxygenase-1: unleashing the protective properties of heme. *Trends Immunol*. 2003;24(8):449–455.
30. Otterbein LE, May A, Chin BY. Carbon monoxide increases macrophage bacterial clearance through Toll-like receptor (TLR)4 expression. *Cell Mol Biol (Noisy-le-grand)*. 2005;51(5):433–440.
31. Soares MP, Bach FH. Heme oxygenase-1: from biology to therapeutic potential. *Trends Mol Med*. 2009;15(2):50–58.
32. Chung SW, Liu X, Macias AA, Baron RM, Perrella MA. Heme oxygenase-1-derived carbon monoxide enhances the host defense response to microbial sepsis in mice. *J Clin Invest*. 2008;118(1):239–247.
33. Chora AA, et al. Heme oxygenase-1 and carbon monoxide suppress autoimmune neuroinflammation. *J Clin Invest*. 2007;117(2):438–447.
34. Pae HO, Lee YC, Chung HT. Heme oxygenase-1 and carbon monoxide: emerging therapeutic targets in inflammation and allergy. *Recent Pat Inflamm Allergy Drug Discov*. 2008;2(3):159–165.
35. Sarady JK, et al. Carbon monoxide protection against endotoxic shock involves reciprocal effects on iNOS in the lung and liver. *FASEB J*. 2004;18(7):854–856.
36. Tenhunen R, Marver HS, Schmid R. The enzymatic conversion of heme to bilirubin by microsomal heme oxygenase. *Proc Natl Acad Sci U S A*. 1968;61(2):748–755.
37. Larsen R, et al. A central role for free heme in the pathogenesis of severe sepsis. *Sci Transl Med*. 2010;2(51):51ra71.
38. Motterlini R, Otterbein LE. The therapeutic potential of carbon monoxide. *Nat Rev Drug Discov*. 2010;9(9):728–743.
39. Desmard M, et al. A carbon monoxide-releasing molecule (CORM-3) exerts bactericidal activity against Pseudomonas aeruginosa and improves survival in an animal model of bacteraemia. *FASEB J*. 2009;23(4):1023–1031.
40. Chin BY, Otterbein LE. Carbon monoxide is a poison... to microbes! CO as a bactericidal molecule. *Curr Opin Pharmacol*. 2009;9(4):490–500.
41. Camhi SL, Alam J, Otterbein L, Sylvester SL, Choi AM. Induction of heme oxygenase-1 gene expression by lipopolysaccharide is mediated by AP-1 activation. *Am J Respir Cell Mol Biol*. 1995;13(4):387–398.
42. Wegiel B, et al. Heme oxygenase-1 derived carbon monoxide permits maturation of myeloid cells. *Cell Death Dis*. 2014;5:e1139.
43. Rahman MN, et al. Structural characterization of human heme oxygenase-1 in complex with azole-based inhibitors. *J Inorg Biochem*. 2010;104(3):324–330.
44. Wegiel B, Hanto DW, Otterbein LE. The social network of carbon monoxide in medicine. *Trends Mol Med*. 2013;19(1):3–11.

45. Descamps D, et al. Toll-like receptor 5 (TLR5), IL-1β secretion, and asparagine endopeptidase are critical factors for alveolar macrophage phagocytosis and bacterial killing. *Proc Natl Acad Sci U S A*. 2012;109(5):1619–1624.
46. Hou Z, Falcone DJ, Subbaramaiah K, Dannenberg AJ. Macrophages induce COX-2 expression in breast cancer cells: role of IL-1beta autoamplification. *Carcinogenesis*. 2011;32(5):695–702.
47. Lee KS, Scanga CA, Bachelder EM, Chen Q, Snapper CM. TLR2 synergizes with both TLR4 and TLR9 for induction of the MyD88-dependent splenic cytokine and chemokine response to Streptococcus pneumoniae. *Cell Immunol*. 2007;245(2):103–110.
48. Dziarski R, Gupta D. Role of MD-2 in TLR2- and TLR4-mediated recognition of Gram-negative and Gram-positive bacteria and activation of chemokine genes. *J Endotoxin Res*. 2000;6(5):401–405.
49. Yoshimura A, Lien E, Ingalls RR, Tuomanen E, Dziarski R, Golenbock D. Cutting edge: recognition of Gram-positive bacterial cell wall components by the innate immune system occurs via Toll-like receptor 2. *J Immunol*. 1999;163(1):1–5.
50. Chin BY, et al. Hypoxia-inducible factor 1α stabilization by carbon monoxide results in cytoprotective preconditioning. *Proc Natl Acad Sci U S A*. 2007;104(12):5109–5114.
51. Zuckerbraun BS, et al. Carbon monoxide signals via inhibition of cytochrome c oxidase and generation of mitochondrial reactive oxygen species. *FASEB J*. 2007;21(4):1099–1106.
52. Zhou R, Yazdi AS, Menu P, Tschopp J. A role for mitochondria in NLRP3 inflammasome activation. *Nature*. 2011;469(7329):221–225.
53. Ghiringhelli F, et al. Activation of the NLRP3 inflammasome in dendritic cells induces IL-1beta-dependent adaptive immunity against tumors. *Nat Med*. 2009;15(10):1170–1178.
54. Zheng LM, Zychlinsky A, Liu CC, Ojcius DM, Young JD. Extracellular ATP as a trigger for apoptosis or programmed cell death. *J Cell Biol*. 1991;112(2):279–288.
55. Kawano A, et al. Involvement of P2X4 receptor in P2X7 receptor-dependent cell death of mouse macrophages. *Biochem Biophys Res Commun*. 2012;419(2):374–380.
56. D'Amico G, Lam F, Hagen T, Moncada S. Inhibition of cellular respiration by endogenously produced carbon monoxide. *J Cell Sci*. 2006; 119(pt 11):2291–2298.
57. Gombault A, Baron L, Couillin I. ATP release and purinergic signaling in NLRP3 inflammasome activation. *Front Immunol*. 2012;3:414.
58. Dong DL, et al. Carbon monoxide stimulates the Ca2(+)-activated big conductance k channels in cultured human endothelial cells. *Hypertension*. 2007;50(4):643–651.
59. Williams SE, et al. Hemoxygenase-2 is an oxygen sensor for a calcium-sensitive potassium channel. *Science*. 2004;306(5704):2093–2097.
60. Medzhitov R. Recognition of microorganisms and activation of the immune response. *Nature*. 2007;449(7164):819–826.
61. Janeway CA, Janeway CA Jr, Medzhitov R. Innate immune recognition. *Annu Rev Immunol*. 2002;20:197–216.
62. Fujita T, et al. Paradoxical rescue from ischemic lung injury by inhaled carbon monoxide driven by derepression of fibrinolysis. *Nat Med*. 2001;7(5):598–604.
63. Iyer SS, et al. Necrotic cells trigger a sterile inflammatory response through the Nlrp3 inflammasome. *Proc Natl Acad Sci U S A*. 2009;106(48):20388–20393.
64. Nakamura H, Yamato I, Anraku Y, Lemieux L, Gennis RB. Expression of cyoA and cyoB demonstrates that the CO-binding heme component of the Escherichia coli cytochrome o complex is in subunit I. *J Biol Chem*. 1990;265(19):11193–11197.
65. Hedl M, Abraham C. Distinct roles for Nod2 protein and autocrine interleukin-1beta in muramyl dipeptide-induced mitogen-activated protein kinase activation and cytokine secretion in human macrophages. *J Biol Chem*. 2011;286(30):26440–26449.
66. Kanangat S, et al. Effects of cytokines and endotoxin on the intracellular growth of bacteria. *Infect Immun*. 1999;67(6):2834–2840.
67. Yang J, et al. Flagellins of Salmonella Typhi and nonpathogenic Escherichia coli are differentially recognized through the NLRC4 pathway in macrophages. *J Innate Immun*. 2014;6(1):47–57.
68. Wegiel B, et al. Cell surface biliverdin reductase mediates biliverdin-induced anti-inflammatory effects via PI3K and AKT. *J Biol Chem*. 2009;284(32):21369–21378.
69. Bilban M, et al. Carbon monoxide orchestrates a protective response through PPARγ. *Immunity*. 2006;24(5):601–610.
70. Mamiya T, et al. Hepatocyte-specific deletion of heme oxygenase-1 disrupts redox homeostasis in basal and oxidative environments. *Tohoku J Exp Med*. 2008;216(4):331–339.
71. Long C, Wang Y, Herrera AH, Horiuchi K, Walcheck B. In vivo role of leukocyte ADAM17 in the inflammatory and host responses during E. coli-mediated peritonitis. *J Leukoc Biol*. 2010;87(6):1097–1101.
72. Hoetzenecker W, et al. ROS-induced ATF3 causes susceptibility to secondary infections during sepsis-associated immunosuppression. *Nat Med*. 2012;18(1):128–134.